Adaptive Zigzag Mapping of a Patchy Field by a Long-Range Autonomous Underwater Vehicle

Yanwu Zhang, *Senior Member, IEEE*, Brett W. Hobson, *Member, IEEE*, Brian Kieft, *Member, IEEE*, Michael A. Godin, Thomas Ravens, and Michael Ulmgren

***Abstract*—Spatial heterogeneity and temporal evolution are intrinsic features of some important oceanic processes, e.g., harmful algal blooms and oil spills, where aggregations of organisms or materials are localized and noncontinuous. In a sparse patchy field, routine lawnmower-mode or zigzag surveys by ships or autonomous platforms are not efficient since a large proportion of the survey time is spent on no-patch areas. We developed an adaptive zigzag algorithm for an autonomous underwater vehicle (AUV) to map patchy fields more efficiently than routine zigzag surveys. An AUV autonomously detects the peak and the edge of a patch, and accordingly determines when to turn onto the next zigzag leg. The AUV sweeps through the field on successive zigzag legs. Using an oil spill model data set, the performance of adaptive zigzag surveys is compared with that of routine zigzag surveys. In April 2022, the algorithm was tested on a long-range AUV through a 16-h survey in Monterey Bay, CA, USA, by reading the oil spill model data as the virtual measurement in real time.**

***Index Terms*—Autonomous underwater vehicle (AUV), edge, mapping, oil spill, patch, peak.**

I. Introduction

SPATIAL heterogeneity and temporal evolution are intrinsic features of some important oceanic processes, such as harmful algal blooms (HABs) and oil spills. Physical and biological processes drive the formation of plankton patches [1]. In oil spills, patchiness is driven by submesoscale processes [2]. In a dynamic patchy field, aggregations of organisms or materials are localized, noncontinuous, and migrating. Remote sensing and in situ surveys of the patchy fields are essential for scientific studies and hazard mitigation. Autonomous underwater vehicles (AUVs) have been deployed for surveying subsurface oil patches [3], [4], [5] utilizing their mobile sensing capacities and onboard intelligence.

An AUV can survey a spatial field on preprogrammed grid tracks (i.e., lawnmower mode) [6] or zigzag tracks [7]. However, in a sparse patchy field, such fixed patterns are not efficient since a large proportion of the survey time is spent on no-patch areas. Adaptive methods have been developed to improve search and survey efficiency. In [8], an AUV autonomously located and tracked phytoplankton patches using a gradient-search algorithm. It is observed that moths adopt zigzag-like flight paths upwind in search of an odor source [9]. Olfactory-based AUV search algorithms were designed for tracing chemical plumes. The vehicle achieves detection when the measurement exceeds a preset threshold and then makes turns with a certain pattern to remain in or reacquire the plume [10], [11], [12].

In this article, we consider mapping a field of distributed patches and tracking the patches' evolution over time, which is desired in investigations of oil spills, HABs, and other patchy and dynamic fields. Detecting and mapping many disjoint patches in a field, rather than tracing a single patch, presents a design challenge of not only detecting individual patches but also exploring the broad field. We developed a method for an AUV to detect and map distributed patches on adaptive zigzag transects through the field.

The rest of this article is organized as follows. The algorithm is presented in Section II. Simulation tests and performance comparisons with routine zigzag surveys are given in Section III. The algorithm was tested on a long-range AUV (LRAUV) in a field experiment in Monterey Bay, CA, USA, as reported in Section IV. Finally, Section V concludes this article.

II. Adaptive Zigzag Algorithm

An AUV maps the patchy field through zigzag transects (in the horizontal dimension) on sawtooth (i.e., yo-yo) profiles (in the vertical dimension). The adaptive zigzag algorithm comprises two parallel behaviors. 1) In the vertical dimension: extracting the maximum signal value on each descent or ascent yo-yo profile, i.e., the per-yo-yo maximum. 2) In the horizontal dimension: adaptive zigzags based on the detection of patch peaks and edges. The AUV locates the patch peak out of per-yo-yo maxima of successive yo-yo profiles and locates the patch edge where the signal drops below a threshold percentage of the patch peak.

Manuscript received 19 January 2023; revised 27 July 2023; accepted 24 November 2023. Date of publication 20 February 2024; date of current version 16 April 2024. This work was supported in part by the David and Lucile Packard Foundation through the Monterey Bay Aquarium Research Institute, in part by the U.S. Department of Homeland Security under Grant Award 2014-ST-061-ML0002-03 with collaborators at the Woods Hole Oceanographic Institution, and in part by the Arctic Domain Awareness Center (a U.S. Department of Homeland Security Center of Excellence) Project "Arctic Oil Spill Modeling" (https://arcticdomainawarenesscenter.org/P12_AOSM) through the University of Alaska. *(Corresponding author: Yanwu Zhang.)*

Associate Editor: B. Thornton.

Yanwu Zhang, Brett W. Hobson, and Brian Kieft are with the Monterey Bay Aquarium Research Institute, Moss Landing, CA 95039 USA (e-mail: yzhang@mbari.org; hobson@mbari.org; bkieft@mbari.org).

Michael A. Godin is with IntuAware, Northampton, MA 01062 USA (e-mail: mike@intuaware.com).

Thomas Ravens is with University of Alaska, Anchorage, AK 99508 USA (e-mail: tmravens@alaska.edu).

Michael Ulmgren is with PND Engineers, Inc., Anchorage, AK 99503 USA (e-mail: mulmgren@pndengineers.com).

Digital Object Identifier 10.1109/JOE.2023.3338694

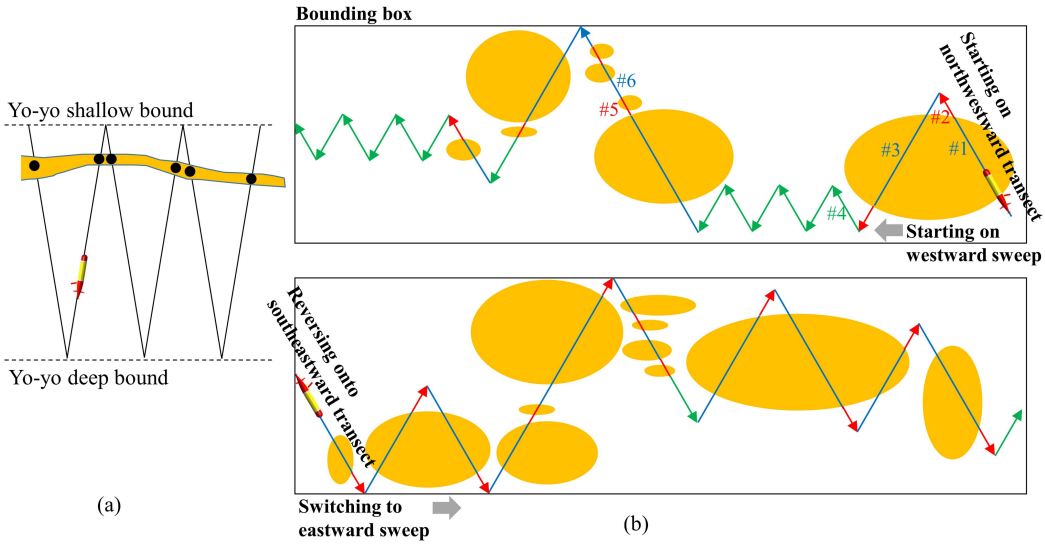

Fig. 1. Illustration of the AUV algorithms for (a) extracting the per-yo-yo maxima (black dots) on successive yo-yo profiles and (b) zigzag tracks through an evolving patchy field. The AUV starts on a westward sweep. When the AUV reaches the northern or southern bound (i.e., if the distance to the bound is less than a specified margin distance), it bounces onto the next leg. When the AUV reaches the western bound, it reverses course to switch to an eastward sweep. The legs with different numbers and color markings are explained in the text.

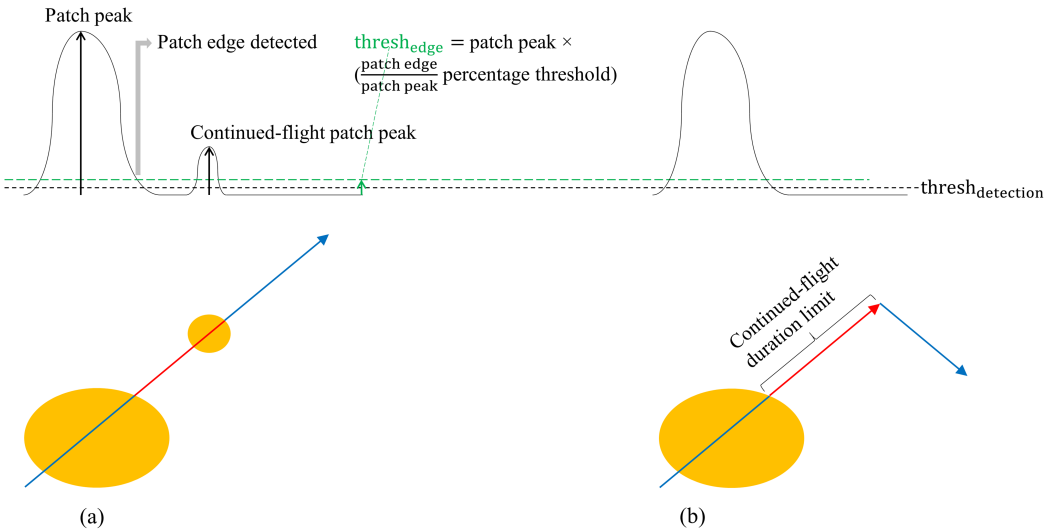

Fig. 2. Illustration of (a) patch edge detection and continued-flight patch detection, and (b) no patch detection on the continued flight. The vehicle's corresponding maneuvers are shown.

A. *Vertical Dimension: Extracting Per-Yo-Yo Maximum*

The AUV extracts the maximum signal value on each descent or ascent yo-yo profile, as shown in Fig. 1(a). The vehicle keeps track of the start and the end of each profile by detecting the vehicle's attitude flip [13] and reports the maximum signal value on completion of that profile. To remove spurious spikes due to sensor noise, the raw measurement goes through a median filter followed by a moving-average lowpass filter [8].

B. *Horizontal Dimension: Adaptive Zigzags Based on Patch Peak and Edge Detections*

The AUV searches for patches on successive zigzag legs, as shown in Fig. 1(b). If the vehicle does not detect any signal above a detection threshold (denoted by $\text{thresh}_{\text{detection}}$ as shown in Fig. 2) after a wait limit (green #4), it makes a turn onto the next zigzag leg. When the AUV transects a patch (blue #1), the signal level rises (on entry into the patch) and then drops (on departure from the patch). The patch peak is picked out of the per-yo-yo maxima on successive yo-yo profiles within a sliding window spanning a certain distance (so that distant peaks are excluded from consideration). When the signal level drops below a threshold percentage of the patch peak, the vehicle declares edge detection and continues flight on the current heading (up to a duration limit) in the hope of finding an adjacent patch. On the continued flight, if the vehicle does not detect a new patch within the continued-flight duration limit (red #2), it makes a turn onto the next zigzag leg (blue #3); but if the vehicle detects a new patch on the continued flight (red #5), it starts a new leg maintaining the current heading (blue #6). The algorithms of edge

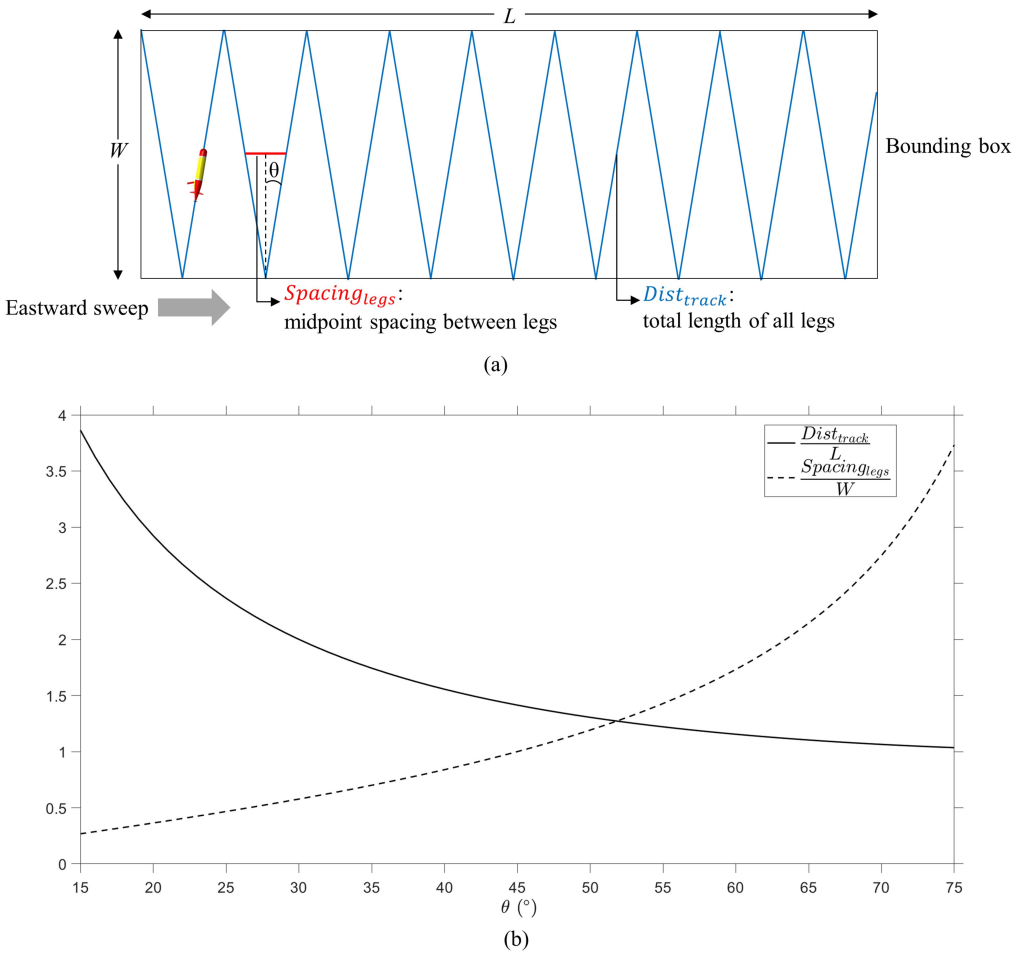

Fig. 3. (a) Hypothetical eastward zigzag sweep through a bounded region of length L and width W for considering the tradeoff between the AUV-traveled distance (colored blue) and the interleg midpoint spacing (color red). (b) Normalized metrics $\mathbf{Dist_{track}}/\boldsymbol{L}$ and $\mathbf{Spacing_{legs}}/\boldsymbol{W}$ as functions of heading $\boldsymbol{\theta}$.

detection and continued-flight patch detection are illustrated in Fig. 2 and explained in Section II-C.

C. Patch Edge Detection and Continued-Flight Patch Detection

The patch edge detection threshold is defined as $\text{thresh}_{\text{edge}} =$ patch peak $\times$ (patch edge/patch peak percentage threshold). As the AUV departs from a patch, when the signal level drops below this threshold, the AUV declares edge detection. Then the vehicle continues flight on the current heading hoping to find an adjacent patch. On the continued flight, if the peak value of a newly detected patch exceeds $\text{thresh}_{\text{edge}}$ of the preceding patch, the vehicle starts a new leg maintaining the current heading [see Fig. 2(a)]. The rationale is: the peak value of the newly detected patch on the continued flight being higher than $\text{thresh}_{\text{edge}}$ (used for edge detection of the preceding patch) is an indication that the patches persist in this direction. Hence it is worthwhile to continue the survey on this heading. If the AUV does not detect any patch above $\text{thresh}_{\text{edge}}$ within the continued-flight duration limit, the vehicle deems it less likely to find new patches in this direction, hence making a turn onto the next zigzag leg [see Fig. 2(b)].

D. Consideration of Sweep Directions and Zigzag Headings

Suppose oil spills are advected by an eastward current, which results in an east–west-oriented swath of patchy field. We accordingly define an east–west oriented box region and let an AUV zigzag through the box on east–west sweeps. This is more efficient than north–south sweeps in a north–south oriented box because the latter would waste some time in no-patch areas to the north or south of the east–west-oriented patchy field. If information about the regional ocean current direction is available, we set the sweep direction to be the same as the anticipated current direction.

When setting the zigzag headings, we need to consider two conflicting requirements. 1) A shorter AUV-traveled distance for faster mapping (at a given vehicle speed). 2) Denser zigzag legs for a higher spatial resolution of mapping. We use a simple hypothetical case of a wall-to-wall zigzag sweep as a benchmark for making these considerations, as shown in Fig. 3. The AUV sweeps through a bounded region of length L and width W. The zigzag legs are symmetric. The heading of the northeastward leg is θ. The zigzag track bounces off the south and north walls. The track distance (i.e., the total length of all legs) of one sweep is: $\text{Dist}_{\text{track}} = L/\sin\theta$. The midpoint spacing between

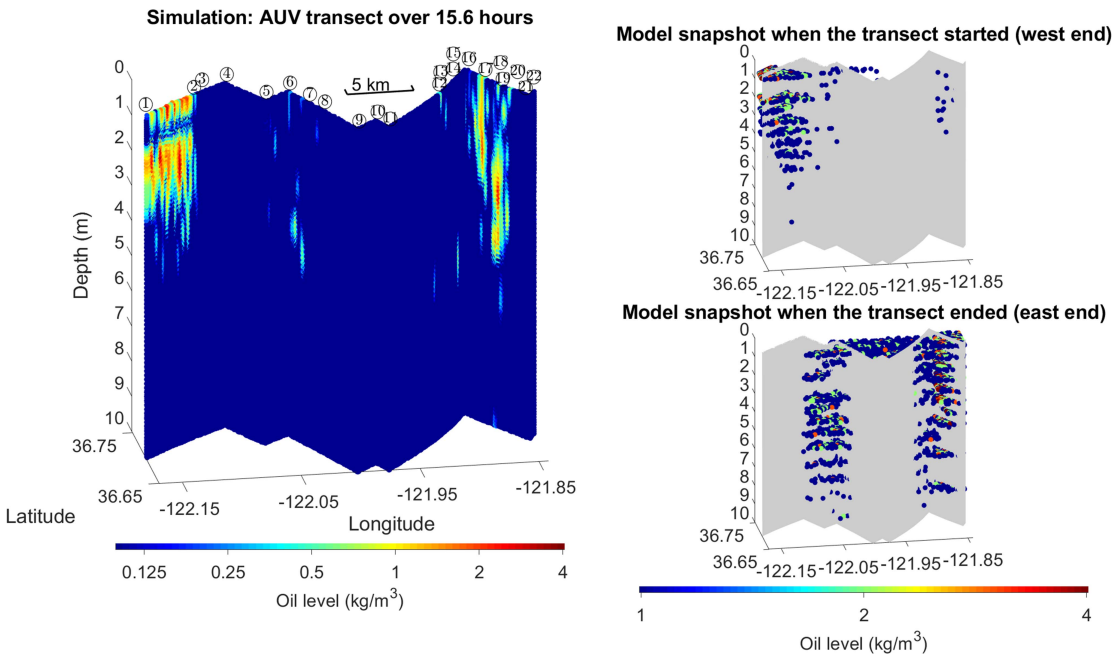

Fig. 4. Oil levels on the AUV's adaptive zigzag transect (left panel) through the oil spill model field (snapshots shown in the right panels) in one simulation test. The AUV's zigzag track is overlaid for reference in the right panels. Latitude and longitude are in degrees.

adjacent legs is: $\text{Spacing}_{\text{legs}} = 2\left((W/2)\tan\theta\right) = W\tan\theta$. We use the ratios $\text{Dist}_{\text{track}}/L = 1/\sin\theta$ and $\text{Spacing}_{\text{legs}}/W = \tan\theta$ as the normalized metrics for assessing the traveled distance and the spatial resolution, respectively. As shown in Fig. 3(b), $\text{Dist}_{\text{track}}/L$ decreases with θ, whereas $\text{Spacing}_{\text{legs}}/W$ increases with θ. A shorter track distance (i.e., faster mapping) calls for a larger θ but a shorter interleg midpoint spacing (i.e., higher spatial resolution) calls for a smaller θ. We set θ to a certain intermediate value to reach a tradeoff between these two conflicting requirements. For example, at $\theta = 30°$, $\text{Dist}_{\text{track}}/L = 2$ and $\text{Spacing}_{\text{legs}}/W = 0.58$. At $\theta = 45°$, $\text{Dist}_{\text{track}}/L = 1.4$ and $\text{Spacing}_{\text{legs}}/W = 1$.

III. Simulation Tests

We test the adaptive zigzag algorithm using an oil spill model data set. The performance of adaptive zigzag surveys is compared with that of routine zigzag surveys.

A. Oil Spill Model Data Set

An oil spill model was developed based on Delft3D software [14] to obtain representative oil concentration data. The model domain was proximal to the Alaska Burger Oilfield in the Chukchi Sea (71.251 °N, 163.195 °W), with an average water depth of 45.5 m [15]. The full model domain extended about 54 km in the east–west direction and 28 km in the north–south direction. Using Delft3D's domain decomposition feature, a 100-m high-resolution grid, extending about 31 km in the east–west direction and 18 km in the north–south direction, was created at the center of the full model domain. Bathymetry data for the model domain was developed based on the International Bathymetric Chart of the Arctic Ocean (IBCAO) v. 3.0 [16]. In the model, it was assumed that the sea was covered by a layer of ice that moved in the northeast direction at a speed of 6 cm/s. Ocean currents traveled easterly with a speed of 10 cm/s. At the start of the simulation, the model assumed that oil had pooled on the underside of the ice, and dissolved oil particles generated by the oil layer were dispersed downward into the water by turbulence (see Fig. 4). The dispersion of the oil particles was modeled using Delft3D's particle tracking feature, and a vertical dispersion coefficient of 8×10^{-4} m^2/s was assumed. The model simulated 120 h with particle generation only in the first 40 h.

For simulating AUV surveys in the oil spill field, the oil spill model data are used to calculate the virtual measurements of the AUV on the survey track. For producing the virtual measurement at time t and location (x, y, z), the following 16 data points surrounding the AUV measurement point (in time and space) are interpolated for generating the virtual measurement:

$$\text{Oil}_{\text{AUV\_virtual}}(x,y,z,t) = M_{\text{interp}} \cdot \begin{bmatrix} \text{Oil}_{\text{model}}(x_0,y_0,z_0,t_0) \\ \text{Oil}_{\text{model}}(x_0,y_0,z_0,t_1) \\ \text{Oil}_{\text{model}}(x_0,y_0,z_1,t_0) \\ \text{Oil}_{\text{model}}(x_0,y_0,z_1,t_1) \\ \text{Oil}_{\text{model}}(x_0,y_1,z_0,t_0) \\ \text{Oil}_{\text{model}}(x_0,y_1,z_0,t_1) \\ \text{Oil}_{\text{model}}(x_0,y_1,z_1,t_0) \\ \text{Oil}_{\text{model}}(x_0,y_1,z_1,t_1) \\ \text{Oil}_{\text{model}}(x_1,y_0,z_0,t_0) \\ \text{Oil}_{\text{model}}(x_1,y_0,z_0,t_1) \\ \text{Oil}_{\text{model}}(x_1,y_0,z_1,t_0) \\ \text{Oil}_{\text{model}}(x_1,y_0,z_1,t_1) \\ \text{Oil}_{\text{model}}(x_1,y_1,z_0,t_0) \\ \text{Oil}_{\text{model}}(x_1,y_1,z_0,t_1) \\ \text{Oil}_{\text{model}}(x_1,y_1,z_1,t_0) \\ \text{Oil}_{\text{model}}(x_1,y_1,z_1,t_1) \end{bmatrix}$$

where $\text{Oil}_{\text{AUV\_virtual}}(x, y, z, t)$ is the AUV virtual measurement at time t and location (x, y, z), and $\text{Oil}_{\text{model}}(x_i, y_j, z_k, t_n)$ is the oil model data at time t_n and location (x_i, y_j, z_k) where

TABLE I
ADAPTIVE ZIGZAG ALGORITHM PARAMETER SETTINGS IN THE SIMULATION TESTS

Bounding box	36.65°N-36.85°N, 121.84°W–122.19°W (22.2 km north–south; 31.2 km east–west)
AUV speed	1 m/s
Yo-yo depth range	0.3–10 m
Zigzag headings	30°/150° on eastward sweep; 330°/210° on westward sweep
$\text{thresh}_{\text{detection}}$	0.1 kg/m^3
Signal-detection wait limit	60 min
$\frac{\text{patch edge}}{\text{patch peak}}$ percentage threshold	10%
Continued-flight duration limit	30 min
Length of sliding window for picking out the patch peak	50 yo-yo profiles (corresponding to 1.9 km distance)
Maximum leg distance	20 km
Margin distance to bounding wall	200 m

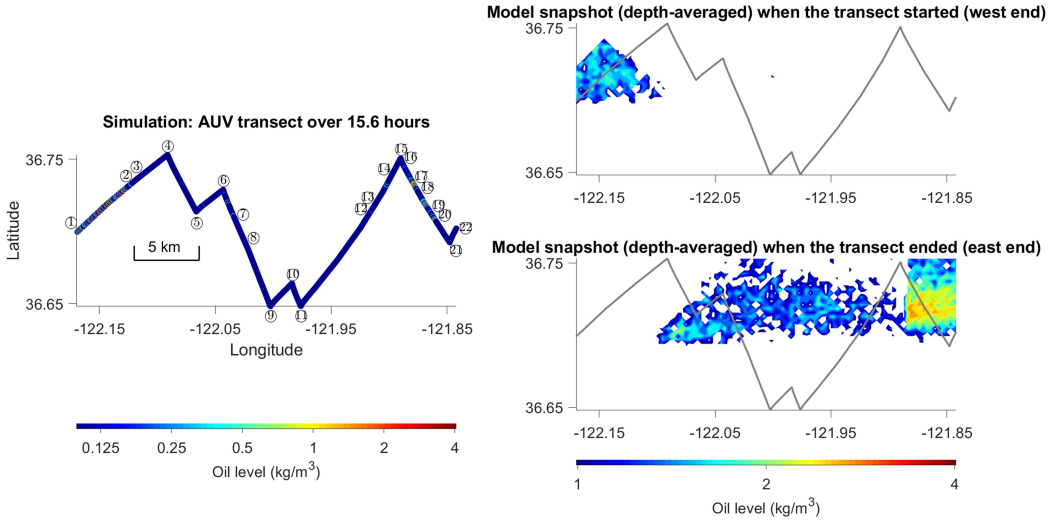

Fig. 5. Plan views of the oil levels on the AUV's zigzag transect (left panel) and the depth-averaged (from 0.3 to 10 m) oil spill model data (right panels) corresponding to Fig. 4. The AUV's zigzag track is overlaid for reference in the right panels. Latitude and longitude are in degrees.

$i, j, k, n = 0$ or 1. The model data points are the nearest points that enclose the AUV virtual measurement location and time: x lies between x_0 and x_1; y lies between y_0 and x_1; z lies between z_0 and z_1; and t lies between t_0 and t_1. M_{interp} is the linear interpolation matrix [17].

B. Parameter Settings

In each test, the AUV reads the virtual measurement (i.e., the interpolated oil spill model data) starting from one day into the model simulation. The parameter settings for the adaptive zigzag algorithm are given in Table I. Based on the geographical size of the oil spill model and the ocean current direction information, we let the AUV run east–west sweeps to map a bounded region of 31 km east–west by 22 km north–south. On an eastward sweep, the headings of the northeastward and the southeastward legs are set to 30° and 150°, respectively, for a reasonable tradeoff between AUV-traveled distance and mapping resolution. On a reverse (i.e., westward) sweep, the headings of the northwestward and the southwestward legs are set to 330° and 210°, respectively. The yo-yo depth range is set to 0.3–10 m.

In the model simulations, we observed that the horizontal scale of individual AUV-transected patches is on the order of a few kilometers. Accordingly, we set the length of the sliding window to 50 yo-yo profiles (corresponding to 1.9 km at 1 m/s

TABLE II
JUNCTION POINTS (MAKING A TURN OR MAINTAINING THE CURRENT HEADING) ON THE ZIGZAG LEGS SHOWN IN FIGS. 4 AND 5

Junction point No. and the associated event	Patch peak value (kg/m^3) versus 1) $\text{thresh}_{\text{detection}}$ = 0.1 kg/m^3 and 2) $\text{thresh}_{\text{edge}}$ of the preceding patch = preceding patch peak value (kg/m^3) × 10% (used only for continued-flight patches)	Next leg heading
① Mission started		30°
② Patch edge detected	Patch peak value 1.6 > 0.1	30°
③ Patch edge detected (continued flight)	Patch peak value 0.25 > 1.6×10%	30°
④ Reached signal-detection wait limit (60 min)	Signal level < 0.1	150°
⑤ Reached signal-detection wait limit (60 min)	Signal level < 0.1	30°
⑥ Reached signal-detection wait limit (60 min)	Signal level < 0.1	150°
⑦ Patch edge detected	Patch peak value 0.25 > 0.1	150°
⑧ Patch edge detected (continued flight)	Patch peak value 0.12 > 0.25×10%	150°
⑨ Reached signal-detection wait limit (60 min)	Signal level < 0.1	30°
⑩ Reached signal-detection wait limit (60 min)	Signal level < 0.1	150°
⑪ Hitting south wall		30°
⑫ Patch edge detected	Patch peak value 0.33 > 0.1	30°
⑬ Patch edge detected (continued flight)	Patch peak value 0.25 > 0.33×10%	30°
⑭ Patch edge detected	Patch peak value 0.26 > 0.1	30°
⑮ Reached continued-flight duration limit (30 min)	Signal level < 0.1	150°
⑯ Patch edge detected	Patch peak value 0.13 > 0.1	150°
⑰ Patch edge detected (continued flight)	Patch peak value 1.1 > 0.13×10%	150°

TABLE II
(CONTINUED)

Junction point No. and the associated event	Patch peak value (kg/m^3) versus 1) $\text{thresh}_{\text{detection}}$ = 0.1 kg/m^3 and 2) $\text{thresh}_{\text{edge}}$ of the preceding patch = preceding patch peak value (kg/m^3) × 10% (used only for continued-flight patches)	Next leg heading
⑱ Patch edge detected	Patch peak value 1.2 > 0.1	150°
⑲ Patch edge detected (continued flight)	Patch peak value 1.4 > 1.2×10%	150°
⑳ Patch edge detected	Patch peak value 0.46 > 0.1	150°
㉑ Reached continued-flight duration limit (30 min)	Signal level < 0.1	30°
㉒ Hitting east wall		210°

speed and 20° pitch angle) for picking out the peak within the horizontal scale of a patch. We set the continued-flight duration limit to 30 min (corresponding to 1.5 km) in the hope of detecting an adjacent qualified patch. In Section V, we discuss the future development of algorithms that will enable an AUV to autonomously adjust these parameters based on real-time statistics learned during mapping.

TABLE III
INITIAL-CONDITION SETTINGS OF THE FOUR PAIRS OF TESTS

	A1/R1	A2/R2	A3/R3	A4/R4
Start latitude	36.7°N	36.7°N	36.8°N	36.8°N
Start heading	30°	150°	30°	150°

C. Simulation Test Example

In the simulation tests, we modified the algorithm: on a leg bouncing from a bounding wall, the AUV maintains heading until detecting signals above $\text{thresh}_{\text{detection}}$ or reaching the maximum leg distance or hitting another bounding wall at which point the vehicle turns onto the next zigzag leg; on a leg not starting from a wall-bounce but preceded by a leg that has encountered a patch, after a wait limit without signal detection, the vehicle turns onto the next zigzag leg. The rationale for the two different treatments is as follows. On a fresh leg starting from a wall-bounce, before encountering any patch, the AUV should maintain the current heading to search for one, because making turns would not increase the likelihood of finding a patch presuming equal likelihood in all directions. However, in the case that the AUV encounters a patch and then continues on the current heading but fails to find an adjacent patch after a certain duration, the vehicle considers it more worthwhile to make a turn in the hope of finding an adjacent patch lateral to the just-encountered patch.

The adaptive zigzag transect in one simulation test is shown in Figs. 4 and 5. Two snapshots of the oil spill model field (at the start and the end of the zigzag transect, respectively) are shown in the right panels of each figure. Over the 15.6-h duration, the oil patches were advected eastward by the ocean current. The AUV captured the patches on the eastward sweep comprising a sequence of zigzag legs. At the junction points between the legs (marked in Figs. 4 and 5, and listed in Table II), the AUV either made a turn or maintained the current heading as detailed below.

The AUV started (point ①) on 30° heading. It then detected a patch with a peak value of 1.6 kg/m^3. When the vehicle departed from the patch and the oil level dropped to

$$\text{thresh}_{\text{edge}} = \text{patch peak} \times \left(\frac{\text{patch edge}}{\text{patch peak}} \text{ percentage threshold} \right) = 1.6\,\text{kg/m}^3 \times 10\% = 0.16\,\text{kg/m}^3$$

the AUV declared edge detection (junction point ②). The vehicle continued flight on 30° heading. On the continued flight, the AUV detected a patch with a peak value of 0.25 kg/m^3. Because 0.25 kg/m^3 > 0.16 kg/m^3 ($\text{thresh}_{\text{edge}}$ of the preceding patch), at this 0.25 kg/m^3 patch's edge (junction point ③) the vehicle started a new leg maintaining the current heading. At junction point ④, when reaching the 60-minute limit without detecting signals above $\text{thresh}_{\text{detection}} = 0.1\,\text{kg/m}^3$, the vehicle made a turn to 150° heading. The zigzag transect continued up to the eastern bound. In the middle of the transect when the vehicle hit the southern bound (junction point ⑪) on 150° heading, it turned to 30° heading back into the bounding box.

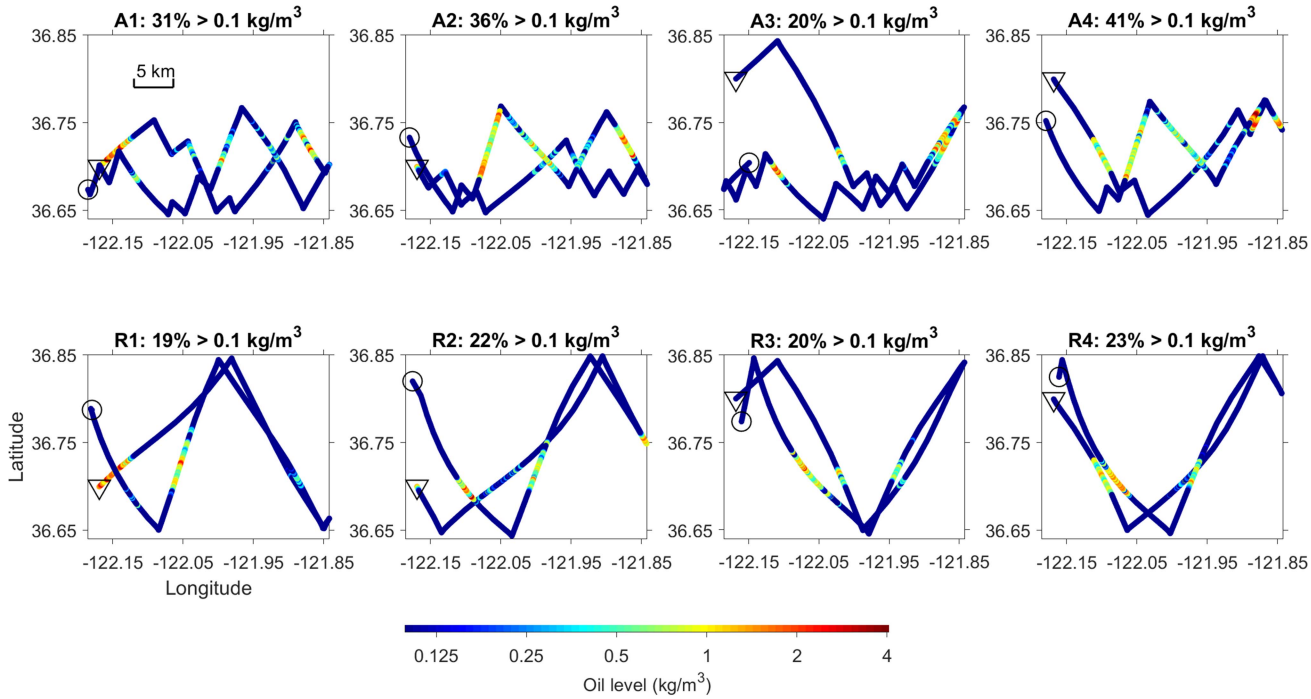

Fig. 6. Performance comparison between adaptive zigzag surveys (upper row; "A" stands for "Adaptive") and routine zigzag surveys (lower row; "R" stands for "Routine") of the simulated oil spill field. The survey duration was 36 h. The start and the end of the survey are marked by the triangle and the circle, respectively. Latitude and longitude are in degrees.

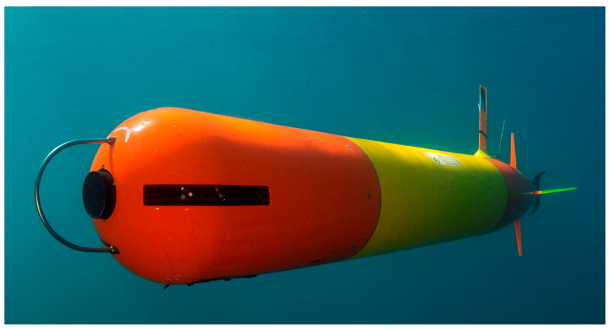

Fig. 7. MBARI LRAUV (photo courtesy of Kip Evans).

D. Performance Comparison Between Adaptive Zigzag and Routine Zigzag Surveys

In a routine zigzag survey, the AUV turns onto the next zigzag leg only when hitting a bounding wall. To compare the performance of adaptive zigzag versus routine zigzag surveys, we ran 4 pairs of tests, as shown in Fig. 6. In each pair of tests, the adaptive zigzag survey is labeled with "A" (e.g., "A1"), and the routine zigzag survey is labeled with "R" (e.g., "R1"). We randomized the tests by altering two initial-condition settings: the AUV's start latitude and heading, as shown in Table III. All of the other parameter settings are kept the same. Over the 36-h mission duration, the AUV swept eastward, hit the eastern bound, and then swept westward.

To evaluate the surveys, we set up an efficiency metric: the percentage of the total traveled distance on which the oil level exceeds the detection threshold ($0.1\,\mathrm{kg/m^3}$). A higher metric value means a larger portion of the AUV track encountered oil spills, thus more efficient. The adaptive zigzag surveys outperformed the routine zigzag surveys in tests 1, 2, and 4, and they tied in test 3, as shown in Fig. 6. The contrast is best shown in test No. 4. On the routine zigzags, the AUV blindly spanned the entire north–south breadth before turning onto the next zigzag leg, hence wasting a large proportion of the survey time on no-patch areas. On the adaptive zigzags, the AUV made timely turns based on patch detection, thus contributing more survey time to patch areas. In the tied test 3, the adaptive zigzags traversed the northern no-patch expanse, thus diminishing the performance gain over the routine zigzags.

IV. Field Test

The LRAUVs developed by the Monterey Bay Aquarium Research Institute (MBARI) are 2.3–3.2 m long (depending on the payload configuration), and have a diameter of 0.3 m at the midsection (see Fig. 7). The LRAUV routinely operates at speeds from 0.5 to 1.2 m/s. The vehicle's depth range is from the surface to 300 m. Using a rechargeable battery, the vehicle can continuously operate for 12 days at 0.8 m/s speed to cover 800 km. Using a primary battery, the vehicle has demonstrated a range of 1800 km (three-week duration) at 1 m/s speed [18]. Its long-range capability is realized by minimizing propulsion power consumption through an innovative design of a low-drag body and a high-efficiency propulsion system [19]. In addition, the vehicle is equipped with a buoyancy engine and is capable of auto-ballasting to neutral buoyancy, which allows flight at a reduced angle of attack to decrease drag. Using the

TABLE IV
PARAMETER SETTINGS IN THE MONTEREY BAY EXPERIMENT

Bounding box	36.68°N–36.80°N, 121.87°W–122.19°W (13.3 km north–south; 28.5 km east–west)
AUV speed	1 m/s
Yo-yo depth range	0.3−10 m
Zigzag headings	30°/150° on eastward sweep
$\text{thresh}_{\text{detection}}$	0.1 kg/m^3
Signal-detection wait limit	90 min
$\frac{\text{patch edge}}{\text{patch peak}}$ percentage threshold	10%
Continued-flight duration limit	60 min
Length of sliding window for picking out the patch peak	50 yo-yo profiles (corresponding to 1.9 km distance)
Maximum leg distance	15 km
Margin distance to bounding wall	200 m

buoyancy engine, the vehicle is also capable of drifting in a lower power state and controlling depth while the thruster is powered OFF. The LRAUV thus combines mobility and speed properties typical of propelled vehicles and the energy savings properties unique to buoyancy-driven vehicles. The vehicle's sensor suite, navigation approaches, and software architecture are introduced in [18].

On April 25, 2022, we deployed LRAUV *Tethys* in Monterey Bay to test the adaptive zigzag algorithm. The parameter settings are given in Table IV.

From the west edge of the bounding box, *Tethys* started the eastward sweep comprising a sequence of zigzag legs, as shown in Figs. 8 and 9. *Tethys* read the interpolated oil spill model data (starting from two days into simulation) as the virtual measurement in real time. Two snapshots of the oil spill model field (at the start and the end of the *Tethys* transect, respectively,) are shown in the right panels in each figure. Over the 16.5-h duration, the oil patches were advected eastward by the ocean current. *Tethys* captured the patches on the eastward sweep. At the junction points between the legs (marked in Figs. 8 and 9, and listed in Table V), *Tethys* either made a turn or maintained the current heading as detailed below.

Tethys started the mission from point ①. Once reaching the zigzag transect beginning waypoint 36.69 °N, 122.17 °W (junction point ②), *Tethys* started the adaptive zigzag on 30° heading. At junction point ③, when reaching the 90-minute limit without detecting signals above $\text{thresh}_{\text{detection}} = 0.1\,\text{kg/m}^3$ *Tethys* made a turn to 150° heading. It then detected a patch with a peak value of 0.97 kg/m^3. At the patch edge (junction point ④), *Tethys* continued flight on 150° heading. When *Tethys* hit the southern bound (junction point ⑤) on 150° heading, it turned to 30° heading back into the bounding box. On the 30° heading, *Tethys* traveled 15 km (the maximum leg distance) without detecting the patch edge because the oil level stayed high and did not fall below 10% of the recent patch peak (i.e., the patch peak within the 1.9-km sliding window), so at junction point ⑥ *Tethys* turned to 150° heading. Then, *Tethys* detected a patch with a peak value of 0.6 kg/m^3. At the patch edge (junction point ⑦), *Tethys* continued flight on 150° heading. On this continued flight, *Tethys* detected a patch with a peak value of 0.17 kg/m^3. Because 0.17 kg/m^3 was higher than the edge threshold of the preceding patch

$$\left(\text{thresh}_{\text{edge}} = \text{patch peak} \times \left(\frac{\text{patch edge}}{\text{patch peak}}\ \text{percentage threshold}\right) = 0.6\,\text{kg/m}^3 \times 10\% = 0.06\,\text{kg/m}^3\right)$$

at the patch edge (junction point ⑧), *Tethys* started a new leg maintaining the current heading. Shortly afterward *Tethys* hit

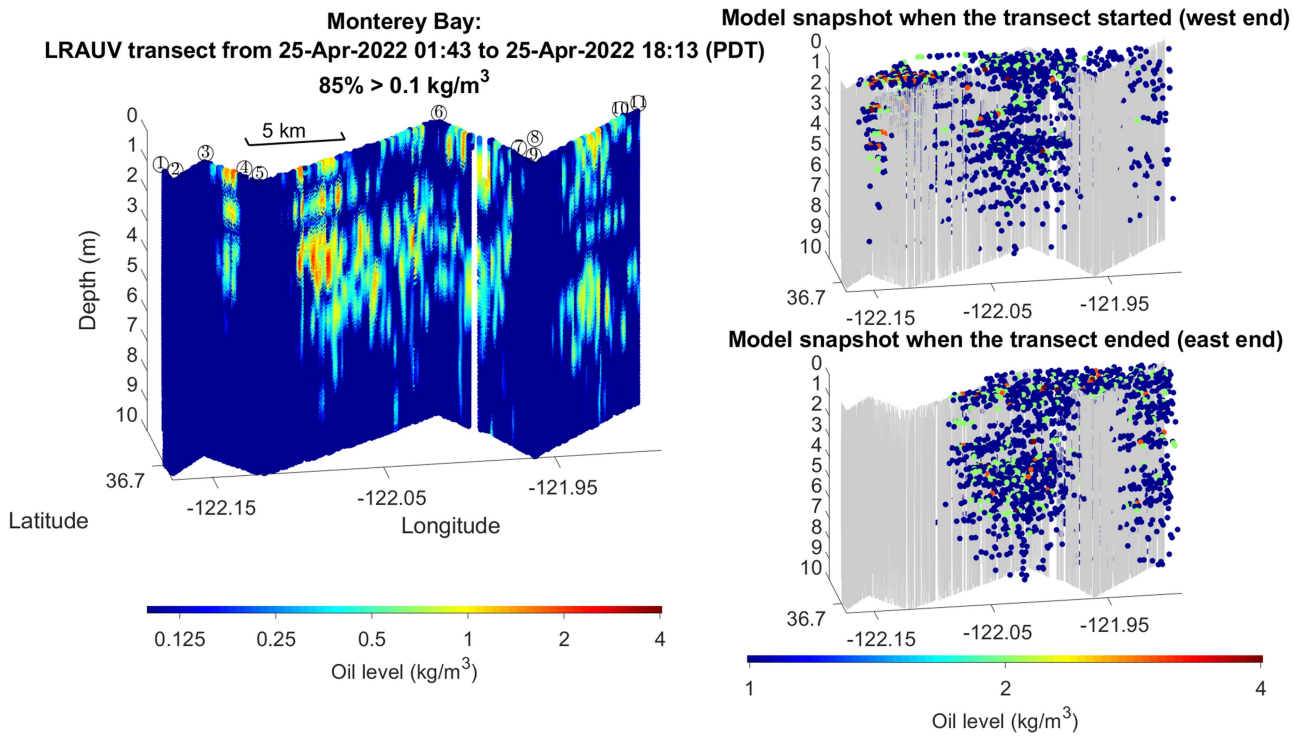

Fig. 8. LRAUV *Tethys* made an adaptive zigzag transect in Monterey Bay (left panel). During this field experiment, *Tethys* was reading the interpolated oil spill model data (right panels) as the virtual measurement in real time. *Tethys'* zigzag track is overlaid for reference in the right panels. Latitude and longitude are in degrees.

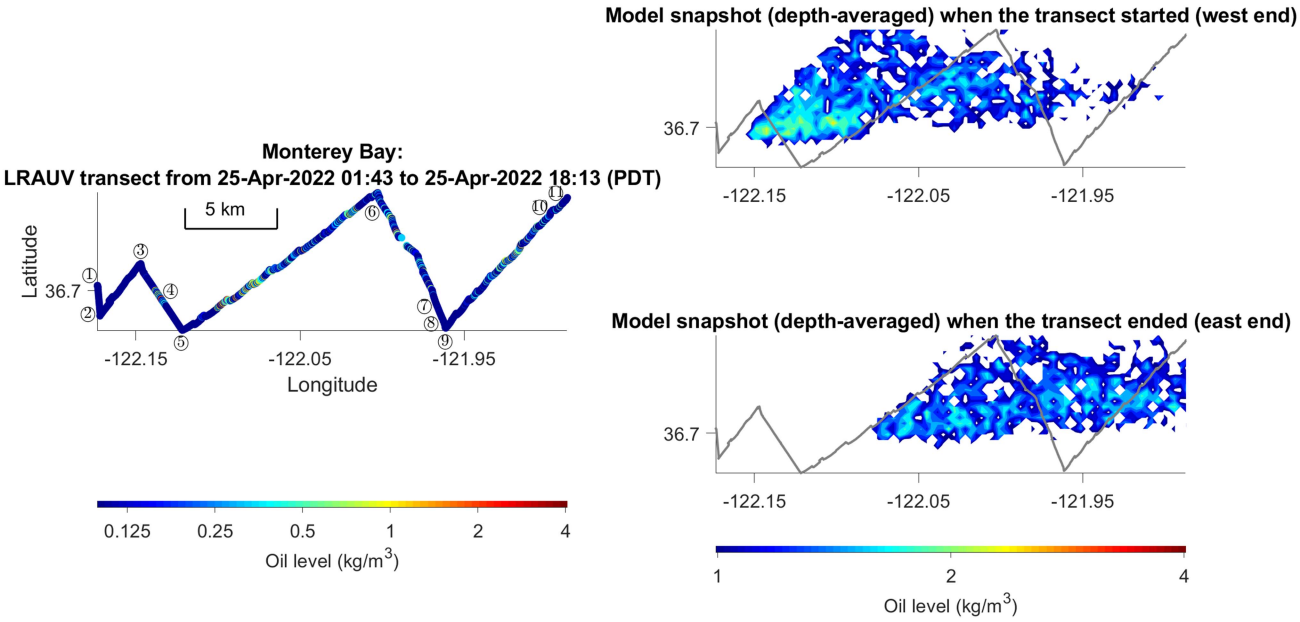

Fig. 9. Plan views of the oil levels on *Tethys'* zigzag transect in Monterey Bay (left panel) and the depth-averaged (from 0.3 to 10 m) oil spill model data (right panels) corresponding to Fig. 8. *Tethys'* zigzag track is overlaid for reference in the right panels. Latitude and longitude are in degrees.

the southern bound (junction point ⑨) and then turned to 30° heading back into the bounding box. Then, *Tethys* detected a patch with a peak value of 0.57 kg/m^3. At the patch edge (junction point ⑩), *Tethys* continued flight on 30° heading until the end of the mission (point ⑪). In this field experiment, the mapping efficiency metric value (i.e., the percentage of the total traveled distance on which the oil level exceeded the detection threshold) was 85%.

V. Conclusion

We developed an AUV adaptive zigzag algorithm for detecting and mapping disjoint patches in a field. In a set of simulation

TABLE V
JUNCTION POINTS (MAKING A TURN OR MAINTAINING THE CURRENT HEADING) ON THE ZIGZAG LEGS SHOWN IN FIGS. 8 AND 9

Junction point No. and the associated event	Patch peak value (kg/m^3) versus 1) $\text{thresh}_{\text{detection}}$ = 0.1 kg/m^3 and 2) $\text{thresh}_{\text{edge}}$ of the preceding patch = preceding patch peak value (kg/m^3) × 10% (used only for continued-flight patches)	Next leg heading
① Mission started		
② Reached waypoint to start the adaptive zigzag transect		30°
③ Reached signal-detection wait limit (90 min)	Signal level < 0.1	150°
④ Patch edge detected	Patch peak value 0.97 > 0.1	150°
⑤ Hitting south wall (continued flight)		30°
⑥ Reached maximum leg distance without detecting patch edge	Patch peak value 0.72 > 0.1	150°
⑦ Patch edge detected	Patch peak value 0.6 > 0.1	150°
⑧ Patch edge detected (continued flight)	Patch peak value 0.17 > 0.6×10%	150°
⑨ Hitting south wall		30°
⑩ Patch edge detected	Patch peak value 0.57 > 0.1	30°
⑪ Mission ended		

tests using an oil spill model data set, the algorithm outperformed routine zigzag surveys in terms of an efficiency metric. The algorithm was tested on an MBARI LRAUV through a 16-h survey in Monterey Bay, by using the oil spill model data as the virtual measurement. This field experiment also demonstrated a novel approach to validating algorithms progressing from simulations to actual sea conditions.

We will improve the algorithm in the following aspects.

A. Adaptive Parameter Settings

In the current algorithm, the sliding window size and the continued-flight duration limit are preset based on the horizontal scale of individual AUV-transected patches in model simulations. In field experiments, the actual features of the patches (e.g., spatial scale, distance between adjacent patches) may differ from the model. We need to develop an adaptive algorithm that starts patch mapping with certain initial settings but learns the patches' statistics on the fly and accordingly adjusts the parameters in real time. For example, the continued flight duration will be adjusted based on the accumulated data of distances between adjacent patches transected by the AUV. The ocean current direction can be estimated in real time from the discrepancy between the AUV's dead-reckoned track and the periodic surface GPS fixes, and used for adjusting the zigzag sweep direction.

B. Supplementary Search Patterns

Desert ants and male moths take spiral paths to search for the nest entrance [20] and intercept the pheromone filaments [21], [22], [23], respectively. Spiral patterns are effective when searching for targets with unknown directions, and the spiral expands over time to increase area coverage. When running the adaptive zigzag algorithm, if the AUV does not encounter a patch after a certain duration, it can switch to a spiral pattern with radius limits (an upper-limit radius to confine the search area and a lower-limit radius set to the AUV's minimum turning radius) in an attempt to intercept a patch. If no patch is detected up to the upper-limit radius, the AUV resumes the paused zigzag pattern to leave this region and explore new regions. If a patch is detected, the AUV switches to a linear leg across this patch and then continues the zigzag pattern. A spiral pattern centered

at the starting point makes slow radial advancement. Therefore, we need to strike a balance between zigzag and spiral patterns in algorithm design.

ACKNOWLEDGMENT

The authors would like to thank the anonymous reviewers for the helpful comments that improved the quality of this article.

REFERENCES

[1] K. L. Robinson, S. Sponaugle, J. Y. Luo, M. R. Gleiber, and R. K. Cowen, "Big or small, patchy all: Resolution of marine plankton patch structure at micro- to submesoscales for 36 taxa," *Sci. Adv.*, vol. 7, 2021, Art. no. eabk2904.

[2] C. H. Barker et al., "Progress in operational modeling in support of oil spill response," *J. Mar. Sci. Eng.*, vol. 8, 2020, Art. no. 668.

[3] R. Camilli et al., "Tracking hydrocarbon plume transport and biodegradation at deepwater horizon," *Science*, vol. 330, pp. 201–204, 2010.

[4] Y. Zhang et al., "A peak-capture algorithm used on an autonomous underwater vehicle in the 2010 Gulf of Mexico oil spill response scientific survey," *J. Field Robot.*, vol. 28, no. 4, pp. 484–496, 2011.

[5] J. Wilkinson et al., "Oil spill response capabilities and technologies for ice-covered Arctic marine waters: A review of recent developments and established practices," *Ambio*, vol. 46, no. Suppl. 3, pp. S423–S441, 2017.

[6] R. B. Wynn et al., "Autonomous underwater vehicles (AUVs): Their past, present and future contributions to the advancement of marine geoscience," *Mar. Geol.*, vol. 352, pp. 451–468, 2014.

[7] M. T. Issac, S. Adams, N. Bose, C. D. Williams, R. Bachmayer, and T. Crees, "Analysis of horizontal zigzag manoeuvring trials from the MUN Explorer AUV," in *Proc. OCEANS*, 2008, pp. 1–7.

[8] Y. Zhang, M. A. Godin, B. Kieft, B.-Y. Raanan, J. P. Ryan, and B. W. Hobson, "Finding and tracking a phytoplankton patch by a long-range autonomous underwater vehicle," *IEEE J. Ocean. Eng.*, vol. 47, no. 2, pp. 322–330, Apr. 2022.

[9] N. J. Vickers, "Winging it: Moth flight behavior and responses of olfactory neurons are shaped by pheromone plume dynamics," *Chem. Senses*, vol. 31, pp. 155–166, 2006.

[10] J. A. Farell, S. Pang, and W. Li, "Chemical plume tracing via an autonomous underwater vehicle," *IEEE J. Ocean. Eng.*, vol. 30, no. 2, pp. 428–442, Apr. 2005.

[11] A. L. Kukulya et al., "Autonomous chemical plume detection and mapping demonstration results with a COTS AUV and sensor package," in *Proc. OCEANS MTS/IEEE Charleston*, 2018, pp. 1–6.

[12] J. Hwang, N. Bose, H. D. Nguyen, and G. Williams, "Acoustic search and detection of oil plumes using an autonomous underwater vehicle," *J. Mar. Sci. Eng.*, vol. 8, 2020, Art. no. 618.

[13] Y. Zhang, J. G. Bellingham, M. A. Godin, and J. P. Ryan, "Using an autonomous underwater vehicle to track the thermocline based on peak-gradient detection," *IEEE J. Ocean. Eng.*, vol. 37, no. 3, pp. 544–553, Jul. 2012.

[14] J. A. Roelvink and G. K. F. M. Van Banning, "Design and development of DELFT3D and application to coastal morphodynamics," *Oceanogr. Literature Rev.*, vol. 11, no. 42, 1995, Art. no. 925.

[15] K. Frazier and T. Ravens, "Oil beneath Arctic Ice: Predicting under-ice storage capacity as a means to better anticipate oil slick spreading under ice," in *Proc. 18th Int. Cold Regions Eng., 8th Can. Permafrost Conf.*, 2019, pp. 263–270.

[16] M. Jakobsson et al., "The international bathymetric chart of the Arctic Ocean (IBCAO) version 3.0," *Geophys. Res. Lett.*, vol. 39, no. 12, 2012, Art. no. L12609.

[17] G. Dahlquist and Å. Björck, *Numerical Methods in Scientific Computing: Volume I*. Philadelphia, PA, USA: SIAM, 2008, pp. 395–396.

[18] B. Hobson, J. G. Bellingham, B. Kieft, R. McEwen, M. Godin, and Y. Zhang, "Tethys-class long range AUVs - extending the endurance of propeller-driven cruising AUVs from days to weeks," in *Proc. IEEE/OES Auton. Underwater Veh.*, 2012, pp. 1–8.

[19] J. G. Bellingham et al., "Efficient propulsion for the Tethys long-range autonomous underwater vehicle," in *Proc. IEEE/OES Auton. Underwater Veh.*, 2010, pp. 1–7.

[20] M. Müller and R. Wehner, "The hidden spiral: Systematic search and path integration in desert ants, *Cataglyphis fortis*," *J. Comp. Physiol. A*, vol. 175, pp. 525–530, 1994.

[21] N. J. Vickers and T. C. Baker, "Latencies of behavioral response to interception of filaments of sex pheromone and clean air influence flight track shape in *Heliothis virescens* (F.) males," *J. Comp. Physiol. A*, vol. 178, pp. 831–847, 1996.

[22] D. Martinez et al., "Multiphasic *on/off* pheromone signalling in moths as neural correlates of a search strategy," *PLoS One*, vol. 8, 2013, Art. no. e61220.

[23] N. Voges, A. Chaffiol, P. Lucas, and D. Martinez, "Reactive searching and infotaxis in odor source localization," *PLoS Comput. Biol.*, vol. 10, 2014, Art. no. e1004019.

Yanwu Zhang (Senior Member, IEEE) was born in 1969 in Shaanxi Province, China. He received the B.S. degree in electrical engineering and the M.S. degree in underwater acoustics engineering from Northwestern Polytechnic University, Xi'an, China, in 1989 and 1991, respectively, the M.S. degree in electrical engineering and computer science from the Massachusetts Institute of Technology (MIT), Cambridge, MA, USA, in 1998, and the Ph.D. degree in oceanographic engineering from the MIT/Woods Hole Oceanographic Institution (WHOI) Joint Program, Cambridge/Woods Hole, MA, USA, in 2000.

From 2000 to 2004, he was a Systems Engineer working on medical image processing at the General Electric Company Research and Development Center, Niskayuna, NY, USA, and a Senior Digital Signal Processing Engineer working on digital communications at Aware Inc., Bedford, MA, USA. Since December 2004, he has been with the Monterey Bay Aquarium Research Institute (MBARI), Moss Landing, CA, USA. As a Senior Research Engineer, he leads the project of targeted sampling by autonomous vehicles. He contributed to the design of the propellers of the *Tethys*-class long-range autonomous underwater vehicles (AUVs). He designs and codes adaptive sampling algorithms for the *Dorado* and *Tethys* AUVs deployed for marine ecosystem studies. Since 1996, he has participated in a series of field experiments running the *Odyssey* IIB, *Dorado*, and *Tethys* AUVs.

Dr. Zhang is currently an Associate Editor of *Frontiers in Marine Science* in the specialty section of Ocean Observation. He is a member of Sigma Xi. As a Ph.D. student, he was a finalist of the MIT Technology Review Magazine's 100 Young Innovators (TR100) in 1999. In 2018, he was the recipient of the Visiting Fellowship of Antarctic Gateway Partnership from the University of Tasmania, Hobart, TAS, Australia. He was a plenary speaker at the 2020 IEEE OES Autonomous Underwater Vehicle Symposium.

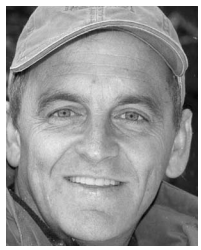

Brett W. Hobson (Member, IEEE) received the B.S. degree in mechanical engineering from San Francisco State University, San Francisco, CA, USA, in 1989.

He began his ocean engineering career with Deep Ocean Engineering, San Leandro, CA, USA, developing remotely operated vehicles. In 1992, he helped start and run Deep Sea Discoveries, where he helped develop and operate deep-towed sonar and camera systems offshore the United States, Venezuela, Spain, and the Philippines. In 1997, he joined Nekton Research, Durham, NC, USA, to develop bioinspired underwater vehicles for Navy applications. After the merging of Nekton Research into iRobot in 2005, he joined the Monterey Bay Aquarium Research Institute, Moss Landing, CA, USA, where he leads the development of the Long-Range Autonomous Underwater Vehicles. He has been the PI or Co-PI on numerous ONR, NSF, DHS, and NASA projects to develop and operate various subsea vehicles for ocean science.

Brian Kieft (Member, IEEE) received the B.S. degree in computer science from Hope College, Holland, MI, USA, in 2001.

From 2001 to 2006, he was with the avionics industry, developing and testing subsystems for military aircraft. In 2006, he joined the Monterey Bay Aquarium Research Institute, Moss Landing, CA, USA, as a Software Engineer. He has worked on various platforms, including mooring controllers, benthic instruments, Wave Gliders, and several autonomous underwater vehicles (AUVs) and their associated payloads. Since 2011, he has also been actively involved in updating and teaching the IEEE tutorial "AUV Technology and Application Basics." He also co-chairs the Wave Glider Users Group. Apart from development, he also takes part in mission planning and payload integration for ongoing collaborative field programs and engineering tests. His current research interests include the development of the *Tethys*-class AUV—a long-range, upper-water-column AUV designed primarily for biological sensing.

Michael A. Godin was born in Westfield, MA, USA, in 1968. He received the B.S. degree in mechanical engineering from Worcester Polytechnic Institute, Worcester, MA, USA, in 1991, and the M.S. degree in nuclear engineering from the Massachusetts Institute of Technology (MIT), Cambridge, MA, USA, in 1994.

He worked at the U.S. Department of Energy headquarters, Washington, DC, USA, from 1991 to 1998, first on robotic handling of spent nuclear fuel, and later on program management of nuclear waste cleanup research. From 1998 to 2003, he was with Hydro-Optics, Biology, and Instrumentation Labs (HOBI Labs), Watsonville, CA, USA, on the hardware design, software design, and manufacturing of underwater optical sensors and submersible data loggers. From 2004 to 2012, he was with the Monterey Bay Aquarium Research Institute (MBARI), Moss Landing, CA, USA, where he developed collaboration systems for geographically distributed groups of researchers, tools for spatio-temporal data exploration, and on a new software architecture for implementing state configured layered control on the *Tethys* AUV. Since 2013, he has run IntuAware, Northampton, MA USA, continuing to support the development of the *Tethys* AUV, and since 2014, he has been with CommunicateHealth, Inc., Rockville, MD, USA, developing data-driven and evidence-based web applications for communicating health information.

Thomas Ravens received the Ph.D. degree in civil and environmental engineering from the Massachusetts Institute of Technology (MIT), Cambridge, MA, USA, in 1997.

He is currently a Professor of Civil Engineering with the University of Alaska Anchorage, Anchorage, AK, USA, where he has served since 2007. He developed and validated predictive process-based models of the main Arctic coastal erosion mechanisms—bluff face thaw/slump (thermal denudation) and niche erosion/block collapse (thermal abrasion). He is working to develop these models into design tools for coastal protection, incorporating both thermal and mechanical control mechanisms. Additionally, he is doing research to quantify and communicate the risk (cost) of Arctic coastal flooding and erosion. For example, to estimate the cost of flooding now and in the future, he uses measures of community flood exposure, in conjunction with data on community expenditures on flood mitigation, to estimate the current and future cost of flooding for a given community. He does research in support of the hydrokinetic renewable energy industry. For example, he uses measurements and models to determine the hydrokinetic energy resource at a given location and models to determine the hydraulic and sediment transport impact of energy extraction. His research interests include Arctic coastal processes and engineering including coastal erosion and flooding.

Michael N. Ulmgren was born in Stockholm, Sweden, in 1974. He received the B.S. and M.S. degrees in civil engineering from the University of Alaska Anchorage (UAA), Anchorage, AK, USA, in 2011 and 2014, respectively.

From 2013 to 2016, he was a water resources associate with Michael Baker International. From 2017 to 2020, he was a research professional with UAA and continued to develop the coastal engineering skill set. He conducted hydrodynamic modeling using Delft3D and applied the Coastal Storm Modeling System (CoSMoS) to quantify shoreline retreat in support of research projects on the North Slope of Alaska. He was a co-developer of a bluff erosion/block collapse model used to quantify rates of bluff erosion at Barter Island, AK, USA. Since the fall of 2020, he has been a Senior Coastal Engineer with PND Engineers, Inc., Anchorage, AK, USA. He designs shoreline revetments to protect essential infrastructure in the coastal zone. His work focuses on quantifying essential environmental design parameters for waterfront projects through numerical modeling and semiempirical and empirical methods.